Check for updates

The paraventricular thalamus provides a polysynaptic brake on limbic CRF neurons to sex-dependently blunt binge alcohol drinking and avoidance behavior in mice

Olivia B. Levine [1], Mary Jane Skelly[2,9], John D. Miller[2], Jean K. Rivera-Irizarry[1], Sydney A. Rowson[2], Jeffrey F. DiBerto[3,4], Jennifer A. Rinker[5,6,7], Todd E. Thiele[8], Thomas L. Kash [3,4] & Kristen E. Pleil [1,2 ✉]

Bed nucleus of the stria terminalis (BNST) neurons that synthesize corticotropin-releasing factor (CRF) drive binge alcohol drinking and anxiety. Here, we found that female C57BL/6J mice binge drink more than males and have greater basal BNST^{CRF} neuron excitability and synaptic excitation. We identified a dense VGLUT2 + synaptic input from the paraventricular thalamus (PVT) that releases glutamate directly onto BNST^{CRF} neurons but also engages a large BNST interneuron population to ultimately inhibit BNST^{CRF} neurons, and this polysynaptic PVT^{VGLUT2}-BNST^{CRF} circuit is more robust in females than males. Chemogenetic inhibition of the PVT^{BNST} projection promoted binge alcohol drinking only in female mice, while activation reduced avoidance behavior in both sexes. Lastly, repeated binge drinking produced a female-like phenotype in the male PVT-BNST^{CRF} excitatory synapse without altering the function of PVT^{BNST} neurons per se. Our data describe a complex, feedforward inhibitory PVT^{VGLUT2}-BNST^{CRF} circuit that is sex-dependent in its function, behavioral roles, and alcohol-induced plasticity.

[1] Graduate School of Medical Sciences, Weill Cornell Medicine, Cornell University, New York, NY, USA. [2] Department of Pharmacology, Weill Cornell Medicine, Cornell University, New York, NY, USA. [3] Department of Pharmacology, University of North Carolina-Chapel Hill School of Medicine, Chapel Hill, NC, USA. [4] Bowles Center for Alcohol Studies, University of North Carolina-Chapel Hill School of Medicine, Chapel Hill, NC, USA. [5] Department of Neuroscience, Medical University of South Carolina, Charleston, SC, USA. [6] Department of Psychiatry and Behavioral Sciences, Medical University of South Carolina, Charleston, SC, USA. [7] Charleston Alcohol Research Center, Medical University of South Carolina, Charleston, SC, USA. [8] Department of Psychology and Neuroscience, University of North Carolina, Chapel Hill, NC, USA. [9] Present address: Psychology Department, Iona College, New Rochelle, NY, USA. ✉email: krp2013@med.cornell.edu

Alcohol use disorder (AUD) is highly co-expressed with other neuropsychiatric diseases including anxiety disorders, with women having increased susceptibility to this comorbidity compared to men (61% vs. 35%, respectively)[1]. Binge alcohol drinking is a primary risk factor for the development of these conditions, and females across mammalian species display greater binge drinking and transition from first alcohol use to disease states more quickly than males[2–6]. These initial differences in alcohol sensitivity suggest that the mechanisms underlying early drinking contribute to disease susceptibility and are important targets for intervention[2]. However, there is a relative dearth of studies investigating the mechanisms controlling binge alcohol drinking in females and the sex differences in the expression of this behavior and consequent vulnerability to disease. The bed nucleus of the stria terminalis (BNST) is a hub in the brain circuits underlying anxiety and alcohol/substance use disorders in humans and is highly sexually dimorphic in mammals[7,8]. The BNST is enriched with neurons that synthesize and release corticotropin-releasing factor (CRF), a stress neuropeptide involved in the development and maintenance of anxiety and addictive disorders, and activation of BNST^{CRF} neurons drives binge drinking behavior and produces anxiety[9,10]; however, the identity and organization of upstream excitatory circuits controlling BNST^{CRF} neuron function and its role in alcohol drinking and anxiety are poorly understood. The BNST is anatomically connected to the paraventricular nucleus of the thalamus (PVT), a region likewise implicated in the etiology of alcohol and substance use disorders and associated behaviors including anxiety[11–14]. Human neuroimaging studies have demonstrated a functional connection between the thalamus and BNST that is denser in females than males[7,8] and decreased thalamic projection strength in young individuals with alcohol abuse[15]. These converging lines of evidence suggest that the PVT-BNST projection might contribute to sex-dependent behavior via modulation of BNST^{CRF} neurons. Here, we systematically examined in both sexes the anatomical and functional architecture of the PVT-BNST^{CRF} circuit and its role in binge alcohol drinking and anxiety behaviors, as well as alcohol-induced plasticity.

Results

Greater BNST^{CRF} neuron excitation and alcohol drinking in females

First, we examined the relationship between sex-dependent binge alcohol consumption and BNST^{CRF} neuron excitation. We showed that female C57BL/6J mice consistently consume more alcohol than males using the Drinking in the Dark (DID)[16,17] model of binge drinking (Fig. 1a). Using whole-cell patch-clamp slice electrophysiological recordings in BNST^{CRF} neurons (Fig. 1b), we found that the proportion of BNST^{CRF} neurons active in their basal state was more than twice as high in females compared to males (60% in females vs. 24% in males; Fig. 1c). Further evaluation of BNST^{CRF} neurons in slice showed that the frequency of spontaneous excitatory postsynaptic currents (sEPSCs), including activity-independent "miniature" EPSCs (mEPSCs), was higher in females than males, but the frequency of inhibitory postsynaptic currents (sIPSCs and mIPSCs) was not (Fig. 1d, e; Supplementary Fig. 1). These results suggest that spontaneous glutamate, but not GABA, release onto BNST^{CRF} neurons is greater in females than males, contributing to an overall increased synaptic drive onto BNST^{CRF} neurons in females (biased toward excitation) compared to males (Fig. 1f). To determine whether increased excitability and excitation of BNST^{CRF} neurons may be related to potentiated alcohol intake in females, we assessed the ability of chemogenetic inhibition of BNST^{CRF} neurons to suppress binge alcohol consumption in males and females. By comprehensively analyzing the effects of

sex and agonist dose in a broader dataset from a mixed-sex cohort of mice we previously published[18], we found that females with the hM4D Gi-coupled designer receptor exclusively activated by designer drug (Gi-DREADD) in BNST^{CRF} neurons required a higher dose of CNO (10 mg/kg) to attenuate binge drinking than their male counterparts (3 mg/kg; Supplementary Fig. 2). Together, these data suggest that the level of activity in the BNST^{CRF} neuron population was sufficiently higher in females to necessitate more robust functional inhibition to affect binge drinking behavior.

Robust projection from the paraventricular thalamus modulating BNST^{CRF} neurons

The sex differences in the underlying physiology and excitatory synaptic input to BNST^{CRF} neurons led us to examine whether there are sex differences in the anatomical and/or functional density of specific glutamatergic inputs to the BNST that may modulate BNST^{CRF} neurons. Using a viral retrograde tracing approach in VGLUT2-ires-Cre (VGLUT2-Cre) mice to label VGLUT2-positive (VGLUT2+) and negative (VGLUT2-) BNST-projecting neurons (Fig. 2a), we identified several known sources of excitatory input to the BNST, including a well-characterized input from the basolateral amygdala (BLA) shown to reduce avoidance behavior in males[19,20]. We found that the brain region with the densest projection to the BNST was the PVT, which was similarly robust in both sexes across the anterior-posterior extent of the PVT and enriched in the anterior-mid PVT (Fig. 2b,d–e; Supplementary Fig. 3a–d). Nearly all labeled neurons in the PVT were VGLUT2+ (Fig. 2c; Supplementary Fig. 3e), indicating a nearly pure glutamatergic projection, consistent with the literature showing that most PVT neurons are glutamatergic[21–24]. To determine whether PVT^{VGLUT2} neurons play a role in binge drinking behavior, we injected a Cre-dependent virus expressing the kappa opioid receptor (KOR)-based Gi-DREADD (Gi-KORD)[25] or control (CON) virus into the PVT of VGLUT2-Cre mice (Supplementary Fig. 4a). Following administration of the Gi-KORD ligand Salvinorin B (SalB; 17 mg/kg, s.c.), male and female Gi-KORD mice but not CONs displayed blunted binge drinking behavior (Supplementary Fig. 4b). In contrast, SalB activation of the Gi-KORD did not alter sucrose drinking or avoidance behavior in the open field test (OF; Supplementary Fig. 4c–e), suggesting that PVT^{VGLUT2} neurons drive alcohol binge drinking behavior specifically without altering reward-seeking behavior or anxiety more generally.

We next evaluated sex differences in the function of BNST-projecting PVT (PVT^{BNST}) neurons. Whole-cell patch-clamp recordings of PVT^{BNST} neurons indicated no sex differences in the intrinsic or synaptic excitability of this neuron population apart from decreased sIPSC amplitude in females (Supplementary Fig. 5). To establish whether there are sex differences in the function of the PVT^{BNST} circuit and postsynaptic responses from BNST^{CRF} neurons, we injected a CaMKIIα-driven channelrhodopsin (ChR2) virus into the PVT of CRF-reporter mice and recorded from BNST^{CRF} neurons (Fig. 3a, b). We found that ChR2 activation of the PVT synaptic input (2 ms pulse of 490 nm LED) elicited an optically-evoked monosynaptic EPSC and polysynaptic IPSC (oEPSC and oIPSC, respectively) in BNST^{CRF} neurons, as both currents could be abolished by bath application of the voltage-gated sodium channel blocker tetrodotoxin (TTX, 500 nM) but only the oEPSC was restored by addition of the voltage-gated potassium channel blocker 4-aminopyridine (4-AP, 100 μM; Fig. 3c,d). Investigation of potential sex differences in PVT-BNST^{CRF} excitatory synapses revealed that the paired-pulse ratios of pharmacologically-isolated PVT-evoked oEPSCs in BNST^{CRF}
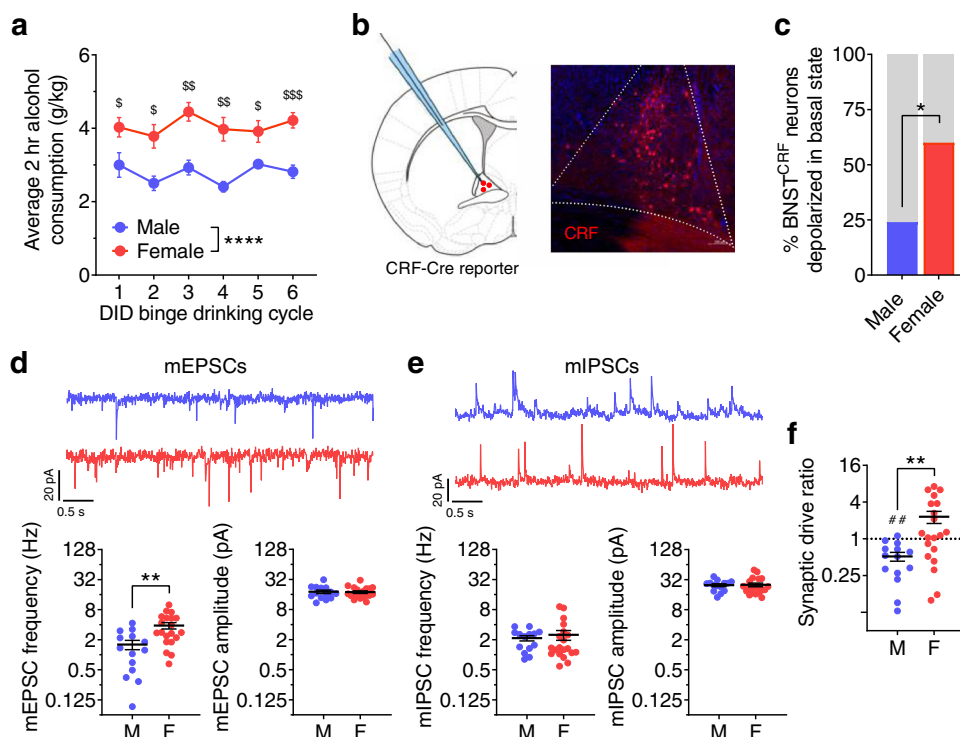
Fig. 1 Females display higher binge alcohol drinking and have greater BNST^{CRF} neuron excitation. a Average 2-h alcohol consumption across cycles of the Drinking in the dark (DID) binge drinking paradigm (N's = 10 M, 10F). 2xRM-ANOVA: main effect of sex ($F_{1,18}$ = 34.81, ****P < 0.0001) and no effect of cycle (P = 0.101) or interaction (P = 0.531); post hoc two-tailed t-tests with Holm-Sidak corrections within-cycle show sex differences on all cycles (C1: t_{17} = 2.41, $^{\$}P$ = 0.032; C2: $t_{14.8}$ = 3.41, $^{\$}P$ = 0.012; C3: $t_{17.1}$ = 4.69, $^{\$\$}P$ = 0.001 C4: $t_{12.4}$ = 4.69, $^{\$\$}P$ = 0.003; C5: $t_{11.3}$ = 2.83, $^{\$}P$ = 0.030; C6: $t_{17.7}$ = 5.06, $^{\$\$\$}P$ = 0.0005). **b**, Schematic of whole-cell patch-clamp recordings of BNST^{CRF} neurons (left) and representative image of a coronal BNST section (right) from a CRF-Cre × Ai9 reporter mouse. **c** Proportion of BNST^{CRF} neurons active in their basal state (Fisher's exact test *P = 0.021, N's = 13 M, 25 cells; 11 F, 25 cells). **d–f** Spontaneous (miniature) excitatory and inhibitory postsynaptic currents (mEPSCs and mIPSCs) in the presence of TTX (1 µM) to block action potential-dependent synaptic transmission in BNST^{CRF} neurons (N's = 3 M, 14 cells; 5 F, 21 cells), compared between males and females using two-tailed unpaired t-tests. **d** Top: representative traces of mEPSCs in BNST^{CRF} neurons of males (blue, above) and females (red, below). Bottom: mEPSC frequency (left, t_{32} = 3.44, **P = 0.002) and mEPSC amplitude (right, t_{32} = 0.06, P = 0.956). **e** Top: representative traces of mIPSCs. Bottom: mIPSC frequency (left, t_{32} = 0.32, P = 0.753) and mIPSC amplitude (t_{32} = 0.13, P = 0.901). **f**, Synaptic drive ratio, calculated as (mEPSC frequency × amplitude)/(mIPSC frequency × amplitude) is higher in females than males (t_{32} = 2.99, **P = 0.005) and below 1.0 in males (one-sample t-test: t_{13} = 4.06, $^{\#\#}P$ = 0.001) but not females (one-sample t-test: t_{19} = 0.83, P = 0.415). Data are presented as mean values ± SEM.

neurons separated by 50 ms were higher in males than females, suggesting a greater probability of evoked presynaptic glutamate release from PVT terminals in the BNST in females (Fig. 3e). In contrast, AMPA/NMDA ratios of oEPSCs were similar between males and females, indicating no postsynaptic sex difference (Fig. 3f). Intriguingly, PPR was below 1.0 in females (Fig. 3e), suggesting that these PVT terminals require relatively little excitation to elicit glutamate release, and thus PVT-BNST^{CRF} synapses may serve as low-pass synaptic filters in females. Further, quantification of oEPSC and oIPSC amplitudes within individual neurons across increasing LED power showed a more robust response in BNST^{CRF} neurons of females compared to males (Fig. 4a, b, Supplementary Fig. 6a, b), providing converging evidence for increased evoked glutamate release from PVT terminals in the BNST. In conjunction with increased spontaneous glutamate release onto BNST^{CRF} neurons in females (Fig. 1, Supplementary Fig. 1), these results suggest higher PVT glutamate tone in the BNST of females than males.

However, oIPSCs were larger than oEPSCs in most individual BNST^{CRF} neurons in both sexes, resulting in a net effect of synaptic inhibition by PVT afferent activation in both males and females (Fig. 4c), similar to what has been described for other limbic projections of the PVT[22–24]. In addition, the latency between optical excitation of PVT terminals and initiation of

oPSCs was significantly longer for oIPSCs than oEPSCs within individual BNST^{CRF} neurons in both sexes (Fig. 4d), providing converging evidence that the PVT-evoked inhibition onto BNST^{CRF} neurons was polysynaptic in nature. These results suggest that increased glutamate release from PVT inputs in females also results in increased polysynaptic inhibition of BNST^{CRF} neurons. We confirmed that activating PVT^{BNST} glutamatergic inputs results in a net hyperpolarization of the membrane potential of BNST^{CRF} neurons using whole-cell current-clamp recordings. LED excitation of ChR2 from PVT terminals produced an optically-evoked postsynaptic potential (oPSP) that was negative (hyperpolarizing) in most BNST^{CRF} neurons in both males and females, regardless of their resting membrane potential (Fig. 4e,f). Evaluation of oPSPs in response to PVT ChR2 excitation across a range of frequencies (Supplementary Fig. 6c,d) showed that 20 Hz stimulation (the same frequency used to evaluate PPR) elicited a greater magnitude second oPSP than the first oPSP in BNST^{CRF} neurons of males but no difference at any frequency in females, consistent with higher PPR in males than females. Thus, while female PVT inputs readily release glutamate, those in males have a lower probability of release but may be more prone to synaptic facilitation upon repeated stimulation, indicating an increased capacity for plasticity.
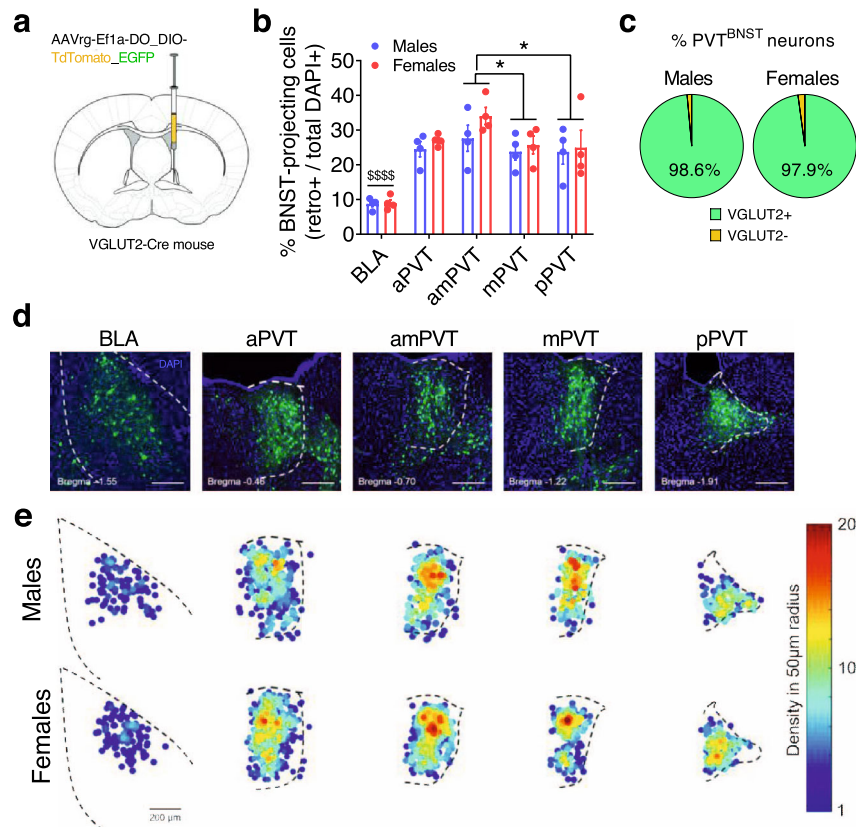
Fig. 2 The PVT provides a dense glutamatergic projection to the BNST. a Viral unilateral retrograde tracing strategy in the BNST of VGLUT2-Cre mice (N's = 4 M, 4 F). **b** % cells in the basolateral amygdala (BLA) and paraventricular nucleus of the thalamus (PVT) sections that project to the BNST (the densest sources of glutamatergic input identified), calculated as (total # of retrogradely-labeled cells/total DAPI+) × 100 and presented as mean values ± SEM. Mixed-effects model: main effect of subregion ($F_{4,23}$ = 32.01, $P < 0.0001$, not indicated) but no effect of sex ($P = 0.967$) or interaction ($P = 0.524$); post-hoc two-tailed t-tests with Holm-Sidak corrections between subregions: BLA has fewer BNST-projecting neurons than the PVT across all A/P coordinates (all $^{\$\$\$\$}Ps < 0.0001$), and that the amPVT has more than the mPVT ($t_{23} = 2.94$, $^*P = 0.037$) and pPVT ($t_{23} = 3.15$, $^*P = 0.027$), with no other differences: aPVT vs. amPVT ($P = 0.085$); aPVT vs. mPVT ($P = 0.873$); aPVT vs. pPVT ($P = 0.873$); mPVT vs. pPVT ($P = 0.873$). aPVT, anterior PVT; amPVT anterior-mid PVT; mPVT, mid PVT: pPVT, posterior PVT. **c** Proportion of VGLUT2-Cre+ (EGFP-labeled) and VGLUT2-Cre− (tdTomato-labeled) BNST-projecting PVT (PVT^{BNST}) neurons in males and females, showing that almost all PVT^{BNST} neurons are VGLUT2+ in both males and females with no difference between sexes (two-tailed unpaired t-test: $t_6 = 1.24$, $P = 0.261$). **d** Representative images of coronal brain slices from a virus-injected mouse illustrating the expression of DAPI (blue) and all BNST-projecting cells (both VGLUT2-Cre + and - in green) in the BLA and across the A/P extent of the PVT. **e** Density heat maps illustrating the average number of BNST-projecting cell bodies within a 50 μM radius of each identified projection neuron for samples from each sex, matched and scaled similarly to representative images in **d** (top: males, bottom: females).

PVT^{BNST} circuit regulation of alcohol drinking and anxiety behaviors. Given the inhibitory effect of ex vivo PVT^{BNST} afferent activation on BNST^{CRF} neuron excitability, we next evaluated the role of the PVT^{BNST} circuit in binge drinking and anxiety-like behavior. We used a multiplexed chemogenetic strategy[25] to bidirectionally and independently manipulate the PVT^{BNST} circuit during behavior by injecting either a cocktail of a Cre-dependent excitatory (hM3D) Gq-DREADD + Cre-dependent inhibitory Gi-KORD or a Cre-dependent CON vector in retrogradely Cre-labeled PVT^{BNST} neurons (Fig. 5a, b; Supplementary Fig. 7). We found that CNO administration (5 mg/kg, i.p.) to activate the Gq-DREADD prior to alcohol access during Day 4 DID did not reliably alter binge consumption of 20% alcohol compared to vehicle baseline (Fig. 5c); however, there was a trend for a decrease in consumption in DREADD males (see Supplementary Fig. 8a), suggesting that activation of the PVT^{BNST} pathway may be sufficient to blunt binge alcohol drinking in a subset of males. In contrast, Salvinorin B (SalB) administration (17 mg/kg, s.c.) to activate the Gi-KORD robustly increased binge alcohol drinking in DREADD females but had no effect in DREADD males or either CON group (Fig. 5d,

Supplementary Fig. 8b), suggesting that tonic activity of the PVT^{BNST} circuit (Supplementary Fig. 5c) engaging interneurons is necessary for active suppression of alcohol drinking behavior in females. As BNST^{CRF} neurons show larger postsynaptic responses to the PVT^{BNST} input in females, reducing the activity of the PVT^{BNST} input may result in more robust disinhibition of BNST^{CRF} neurons to further enhance binge drinking. Intriguingly, neither chemogenetic manipulation affected 1% sucrose consumption in a similar DID paradigm (Supplementary Fig. 8c, d). These results suggest that the PVT^{BNST} projection plays a unique inhibitory role in binge drinking behavior that is not dependent on modulation of the general rewarding or aversive aspects of drug intake and consummatory behavior previously shown to be mediated by other major limbic outputs of the PVT such as the nucleus accumbens[23,26,27].

We also probed whether the PVT^{BNST} circuit plays a role in anxiety-like behavior, given our previous work showing that activity of the BNST^{CRF} neuron population is anxiogenic[18,28] and that the PVT regulates emotional behaviors[14,22]. CNO administration to activate the Gq-DREADD decreased avoidance of the open arms on the elevated plus maze (EPM) in DREADD mice
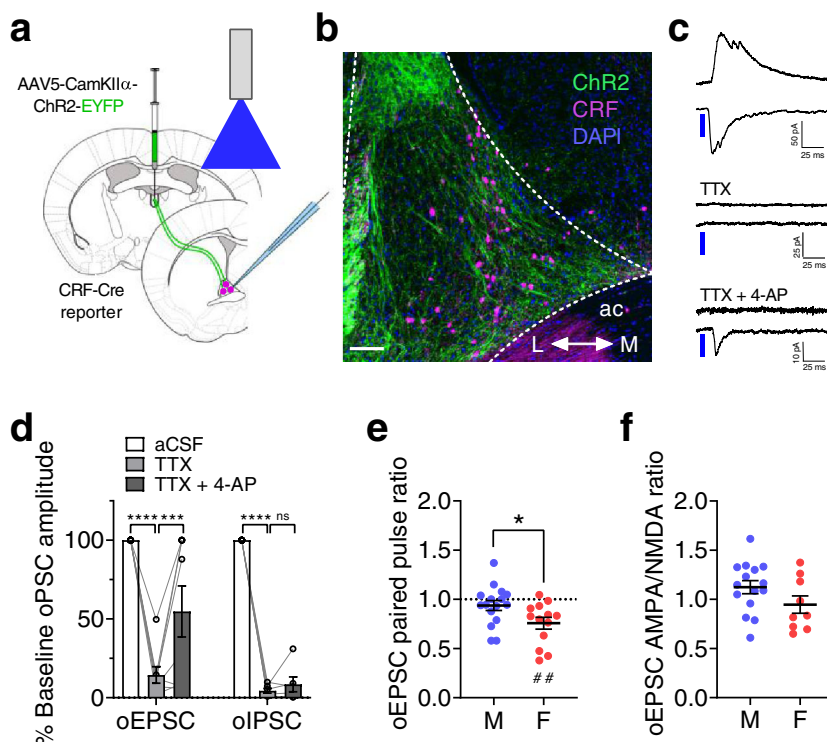
Fig. 3 The PVT-BNST projection provides polysynaptic inhibition onto BNST^{CRF} neurons. a–b Approach for slice recordings in BNST^{CRF} neurons during optical excitation of ChR2 in PVT axon terminals (**a**) and representative coronal image of the dorsal BNST (**b**); ac = anterior commissure, L = lateral, M = medial. Scale bar = 100 μM. Similar images were used to visually confirm ChR2 expression in each round of surgery and produced similar results. **c–d** Representative traces (**c**) and quantification (**d**) of time-locked optically-evoked EPSCs (oEPSCs) and IPSCs (oIPSCs) in BNST^{CRF} neurons in response to 2 ms pulses of blue LED at baseline, in the presence of tetrodotoxin (TTX, 1 μM), and with the addition of 4-aminopyridine (4-AP, 100 μM). oEPSCs: 1xRM-ANOVA effect of drug ($F_{2,14} = 22.6$, $P < 0.0001$), post hoc two-tailed paired t-tests with Holm-Sidak corrections (aCSF vs. TTX: $t_{14} = 6.71$, ****$P < 0.0001$; TTX vs. TTX + 4-AP: $t_{14} = 3.16$, **$P = 0.007$); N = 5 mice, 8 cells. oIPSCs: 1xRM-ANOVA effect of the drug ($F_{2,10} = 429.0$, $P < 0.0001$), post hoc two-tailed paired t-tests with Holm-Sidak corrections (aCSF vs. TTX: $t_{10} = 25.90$, ****$P < 0.0001$; TTX vs. TTX + 4-AP: $t_{10} = 1.10$, $P = 0.299$); N = 4 mice, 6 cells. **e** Paired pulse ratio of pharmacologically-isolated oEPSCs is lower in females than males (two-tailed unpaired t-test: $t_{27} = 2.33$, *$P = 0.028$) and below 1 in females (one-sample t-test: $t_{12} = 4.07$, ##$P = 0.002$) but not males (one-sample t-test: $t_{15} = 2.33$, $P = 0.235$). N's = 4 M, 16 cells; 3 F, 13 cells. **f** oEPSC AMPA/NMDA ratios between sexes (two-tailed unpaired t-test: $t_{22} = 1.61$, $P = 0.121$). N's = 4 M, 15 cells; 3 F, 9 cells. Data are presented as mean values ± SEM.

compared to CON mice (Fig. 5e–g), an anxiolytic effect of Gq-DREADD activation that we replicated in the open field test (OF; Supplementary Fig. 8e,f). In contrast, SalB administration to activate the Gi-KORD did not affect avoidance of the center of the open field (Fig. 5h–j). Together, these results suggest that in an anxiogenic context when BNST^{CRF} neuron activity is high[29,30], activation of the PVT^{BNST} synaptic brake is sufficient to decrease anxiety-like behavior.

Repeated alcohol use produces a female-like phenotype in BNST^{CRF} synapses in males. Finally, we examined the sex-dependent plasticity in this circuit following repeated binge alcohol drinking to understand whether there are changes in the PVT^{VGLUT2}-BNST^{CRF} circuit during withdrawal that could precipitate or contribute to increased disease vulnerability. We found that one day after three cycles of EtOH DID (Fig. 6a), the proportion of BNST^{CRF} neurons in an active state was increased following alcohol exposure in males (Fig. 6b); intriguingly, this proportion was unchanged by a history of alcohol exposure in females, suggesting that basal BNST^{CRF} neuron population-level activity may be near a maximum in naïve females (Fig. 1b;

Fig. 6b) in the absence of a discrete salient stimulus (for example, during an anxiety assay such as EPM here). Alternatively, the population level excitability of BNST^{CRF} neurons in females may be relatively impervious to the effects of extended alcohol exposure. Notably, a range of neural activity patterns was observed in all groups, illustrating the heterogeneity of the BNST^{CRF} population in both sexes as previously described in males[31,32]. Most other measures of intrinsic excitability and current-injected firing were neither different between males and females nor altered following EtOH DID exposure when measured either at their resting membrane potential (RMP; Supplementary Fig. 9) or at a common hyperpolarized potential of −70 mV (Supplementary Fig. 10). This suggests that the primary effect of repeated alcohol exposure on BNST^{CRF} neuron excitability is on the population-level activity, with males developing a female-like phenotype. Examination of synaptic transmission showed that sEPSC frequency was increased in EtOH males but unchanged in females (Fig. 6c), while sEPSC amplitude was unchanged in both sexes (Fig. 6d). This led to an increase in excitatory synaptic drive onto BNST^{CRF} neurons in males but not females (Fig. 6e). In contrast, there were no changes in the frequency, amplitude, or synaptic drive of sIPSCs in either sex (Fig. 6f–h). Assessment of the
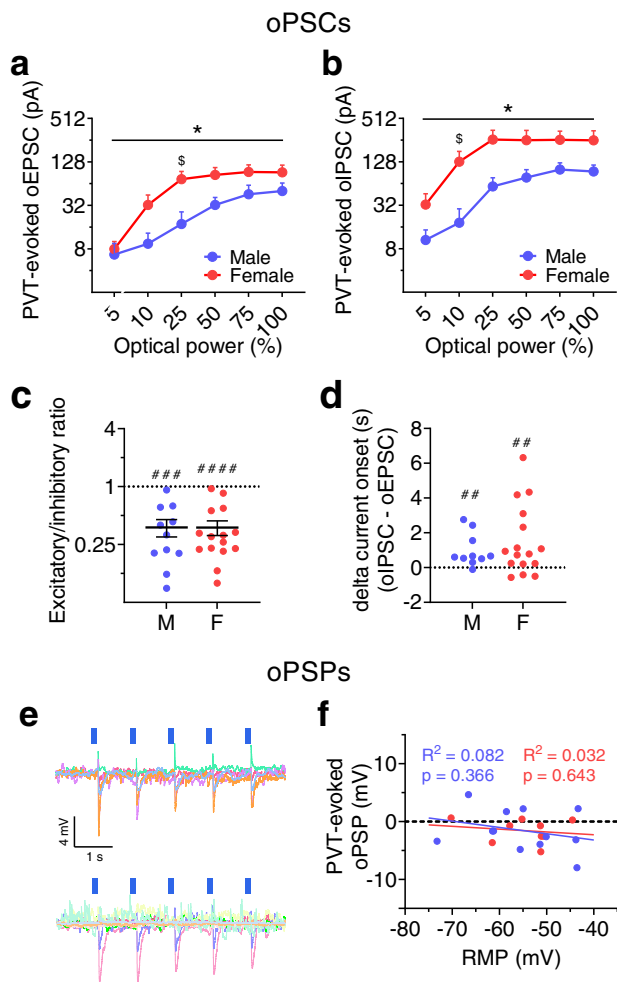
Fig. 4 The PVT provides net inhibition onto BNST^CRF neurons. a–b LED power-response curves for optically-evoked EPSCs (oEPSCs, **a**) and IPSCs (oIPSCs, **b**) in the same BNST^CRF neurons (N's = 2 M, 6 cells; 6 F, 13 cells). Data are presented as mean values + SEM. **a** 2xRM-ANOVA for oEPSCs: power ($F_{5,85} = 48.74$, $P < 0.0001$, not indicated), sex ($P = 0.149$), sex × power interaction ($F_{5,85} = 2.58$, *$P = 0.032$). Post hoc two-tailed *t*-tests with Holm-Sidak corrections reveal a significant difference between males and females for 25% power ($t_{102} = 2.76$, $^{\$}P = 0.041$) but no other LED powers (Ps > 0.55). **b** 2xRM-ANOVA for oIPSCs**:** power ($F_{5,85} = 54.09$, $P < 0.0001$, not indicated), sex ($P = 0.082$), a sex × power interaction ($F_{5,85} = 2.89$, *$P = 0.019$), but no main effect of sex ($P > 0.05$). Post hoc two-tailed *t*-tests with Holm-Sidak corrections reveal a sex difference for 10% power ($t_{102} = 2.94$, $^{\$}P = 0.024$) but no other LED powers (Ps > 0·10). **c** oEPSC/oIPSC ratios in individual BNST^CRF neurons showing net synaptic inhibition (one-sample *t*-tests compared to 1: males: $t_{10} = 5.50$, $^{###}P = 0.0001$; females: $t_{14} = 7.20$, $^{####}P < 0.0001$) with no sex difference (two-tailed unpaired *t*-test: $t_{24} = 0.11$, $P = 0.912$). Data are presented as means ± SEM**. d**, Difference in the onset time of oIPSCs and oEPSCs (one-sample *t*-tests compared to 0: males: $t_9 = 3.32$, $^{##}P = 0.009$; females: $t_{15} = 3.01$, $^{##}P = 0.009$), with no sex difference (two-tailed unpaired *t*-test: $t_{24} = 0.76$, $P = 0.455$). For **c–d**, N's = 5 M, 11 cells; 8 F, 16 cells. **e–f** Optically-evoked postsynaptic potentials (oPSPs) in BNST^CRF neurons from ChR2+ PVT terminals. **e** Overlaid oPSP traces from basally inactive BNST^CRF neurons, with upward deflections indicating time-locked depolarizations and downward deflections indicating hyperpolarizations (males, top; females, bottom). **f** oPSP magnitude plotted as a function of resting membrane potential (RMP). Linear regression equations: males: $Y = -0.109*X - 7.53$; females: $Y = -0.049*X - 4.23$. N's = 7 M, 12 cells; 6 F, 9 cells.

kinetics of sPSCs revealed increased half-width and weighted tau of sEPSCs in EtOH males, consistent with an increase in glutamatergic transmission (Supplementary Fig. 11).

We further examined plasticity in PVT-evoked postsynaptic responses from BNST^CRF neurons and found no significant effect of EtOH on oEPSC raw amplitude across increasing LED power (Fig. 7a). However, when oEPSC amplitude was normalized to maximum within each cell, there was a leftward shift in the power-response curve in males but not females (Supplementary Fig. 12a, b), demonstrating that lower optical power was able to elicit larger oEPSCs in EtOH males compared to controls. Further, analysis of the slope of the initial increase in raw oEPSC amplitude across 5–25% LED power confirmed this alcohol-induced increase in the excitatory postsynaptic responses of BNST^CRF neurons in males (Supplementary Fig. 12c, d), mirroring the alcohol exposure effect on sEPSCs in males (Fig. 6c) and suggesting that PVT-BNST^CRF synapses comprise a large contingent of the glutamate synapses vulnerable to alcohol-induced plasticity. oIPSCs were also somewhat enhanced by alcohol exposure, particularly in males, as analysis of raw oIPSCs across LED power showed a sex × EtOH interaction (Fig. 7b), however, normalized oIPSC amplitude was not significantly altered in BNST^CRF neurons of EtOH mice in either sex (Supplementary Fig. 12e, f); the initial slope was increased in EtOH mice, but this was not significantly different specifically within either sex (Supplementary Fig. 12g, h). Following voluntary alcohol exposure, the E/I ratio of oPSCs remained significantly below 1.0 in males but not females (Fig. 7c), suggesting that while the overall E/I balance toward inhibition was maintained in males (that is, increased PVT-mediated excitation was met with increased polysynaptic inhibition), the net inhibitory effect of PVT afferent activation at BNST^CRF neurons was attenuated in females. However, oEPSC/oIPSC ratios were not different between CON and EtOH females, suggesting that this statistical lack of E/I ratio below one may be due to increased variability in the responses of individual neurons/synapses in females rather than a robust loss of polysynaptic inhibition, Notably, we observed very few sex differences or alcohol-induced changes in the electrophysiological properties, excitability, and synaptic transmission of PVT^BNST neurons themselves (Supplementary Figs. 13 and 14), suggesting that sex-dependent and alcohol-dependent differences in the PVT-BNST^CRF synapse strength are not due to differences in PVT^BNST neuronal excitability per se. Together, our data suggest that the effects of sex and repeated binge alcohol drinking are on the tonic activity of the BNST^CRF neuron population, due to basal differences in and differential plasticity in PVT^VGLUT2-BNST^CRF synapses and BNST^CRF neuron responses to the largely tonically-active PVT^BNST afferents.

Discussion

Altogether, we found that female mice display more robust binge drinking behavior than males and that BNST^CRF neurons are both more tonically active and receive increased excitatory synaptic input in females relative to males. We further demonstrated that the PVT provides a dense excitatory input to the BNST in both sexes[33] that is functionally more robust in females than males, consistent with human neuroimaging studies on thalamic outputs[7,8]. We report that while PVT glutamate neurons directly synapse onto BNST^CRF neurons as recently shown anatomically in males[33], they also provide robust feedforward inhibition of this population by recruiting interneurons, providing a synaptic "brake" on BNST^CRF neuron excitability; such feedforward inhibition has also been reported for other PVT projections, such as those to the nucleus accumbens (NAc) and central
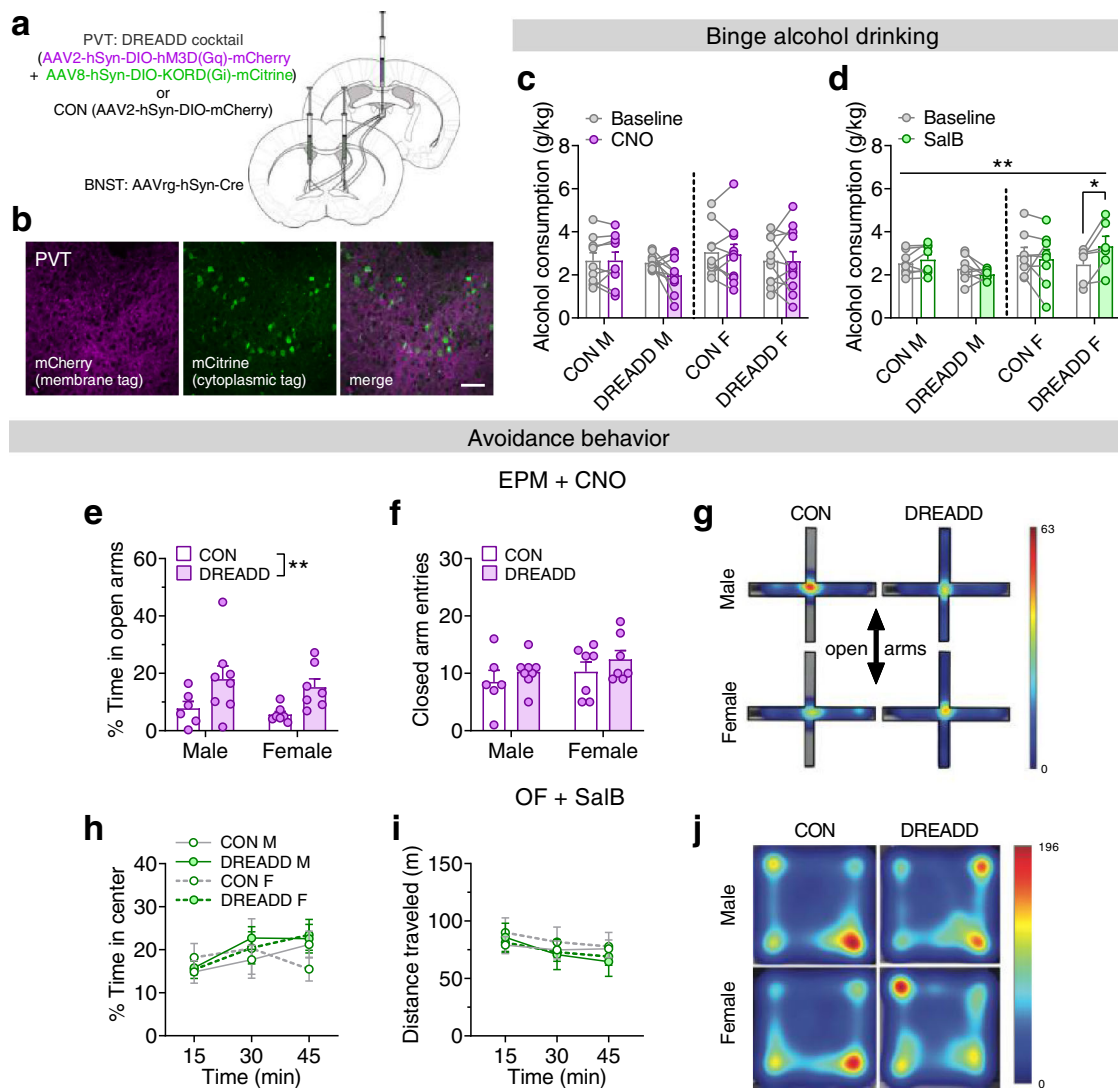
Fig. 5 The PVT^{BNST} projection sex-dependently regulates binge alcohol drinking and avoidance behavior. a Multiplexed chemogenetic approach for PVT^{BNST} neurons. **b** Representative PVT image showing coexpression of the Gq-DREADD (mCherry) and Gi-KORD (mCitrine) in PVT^{BNST} neurons. Scale bar = 50 μM. (Images were acquired for all mice except those used for slice electrophysiology recordings.) **c–d** Alcohol consumption during vehicle baseline vs. Day 4 ligand administration. **c** Clozapine n-Oxide (CNO; 5 mg/kg, i.p.; Gq-DREADD activation). 3xRM-ANOVA: no effects of sex, DREADD, CNO, or any interactions ($Ps > 0.15$; N's = 9 CON M, 11 DREADD M, 10 CON F, 11 DREADD F). **d** Salvinorin B (SalB; 17 mg/kg, s.c.; Gi-KORD activation). 3xRM-ANOVA: sex × DREADD × SalB interaction ($F_{1,26} = 8.76$, **$P = 0.007$) and no main effects and no interactions ($Ps > 0.05$); post hoc two-tailed paired t-tests with Holm-Sidak corrections for effect of SalB: DREADD females ($t_{26} = 3.08$, *$P = 0.019$), all others ($Ps > 0.65$). N's = 8 CON M, 8 DREADD M, 8 CON F, 6 DREADD F, with 0–3 mice/group excluded for below-criteria baseline drinking. **e–g** Effects of CNO on the elevated plus maze (EPM). N's = 6 CON M, 8 DREADD M, 7 CON F, 7 DREADD F. **e** Percent time spent on the open arms. 2xANOVA: main effect of DREADD ($F_{1,24} = 9.30$, **$P = 0.006$) but no other effects ($Ps > 0.45$). Post hoc two-tailed unpaired t-tests with Holm-Sidak corrections within sex ($Ps > 0.05$). **f** Closed arm entries. 2xANOVA: no effects or interaction ($Ps > 0.20$). **g** Representative tracking heat maps. **h–j** Effect of SalB in open field test (OF). N's = 4 CON M, 5 DREADD M, 4 CON F, 5 DREADD F. **h**, Percent time in center. 3xRM-ANOVA: main effect of time ($F_{2,27.6} = 8.70$, $P = 0.003$, not indicated) and no other effects or interactions ($Ps > 0.10$). **i** Distance traveled. 3xRM-ANOVA: main effect of time ($F_{1.2,17.4} = 16.1$, $P = 0.0005$, not indicated) but no other effects or interactions ($Ps > 0.10$). **j** Representative tracking heat maps. Data are presented as mean values ± SEM.

amygdala (CeA)[23,24], to modulate appetitive, drug, and fear-related behaviors in males[22–24,27,34]. For example, the PVT regulates appetitive learning and behavioral responses for the availability of sucrose, food, and water, particularly through its projection to the NAc[35–37]. Intriguingly, we found that inhibition of the entire PVT glutamate neuron population suppressed voluntary, predictable binge drinking behavior (without an effect on palatable binge sucrose consumption using a parallel paradigm; Supplementary Fig. 4), consistent with many of these previously reported complex roles of the PVT in motivated behaviors. In contrast, we found that the PVT^{BNST} circuit plays a

sex-dependent but opposite role in binge alcohol drinking, such that removal of the PVT^{BNST} brake disinhibits alcohol consumption in females without affecting sucrose intake. In contrast, PVT^{BNST} activation may inhibit alcohol consumption in a subset of males, pointing to a difference in the set point for engagement of the PVT-BNST^{CRF} circuit (and thus modulation) between sexes. Our findings provide insight into the mechanisms underlying binge alcohol drinking in females. They also highlight underlying circuit features that are different between males and females, conferring complex sex-dependent control and circuit modulation of binge alcohol consumption. They further point to
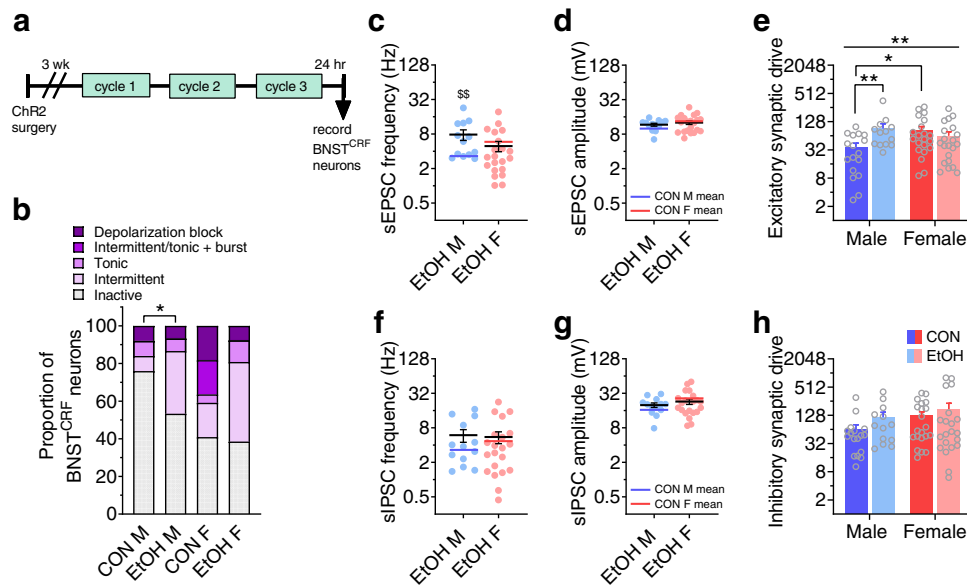
Fig. 6 A history of voluntary binge alcohol drinking induces a female-like phenotype in male BNST^CRF neurons. a Experimental timeline for recording from BNST^CRF neurons one day following three cycles of alcohol DID (EtOH) or water DID control (CON) procedure (means for CON cell data in Fig. 1 are represented in this figure by blue and red lines for CON M and F, respectively). **b** % BNST^CRF neurons in various states of excitability. Chronic alcohol drinking increases the proportion of depolarized neurons in males (Fisher's exact test *$P = 0.037$) but not females ($P > 0.99$). N's = 8 EtOH M, 23 cells; 10 EtOH F, 26 cells. **c–h** Effect of repeated binge alcohol drinking on spontaneous EPSCs and IPSCs in BNST^CRF neurons (N's = 5 EtOH M, 13 cells; 8 EtOH F, 21 cells). **c** sEPSC frequency. Two-tailed unpaired t-tests: males: $t_{28} = 3.08$, $^{\$\$}P = 0.005$; females: $t_{40} = 1.02$, $P = 0.314$. **d** sEPSC amplitude. Two-tailed unpaired t-tests: males: $t_{28} = 1.55$, $P = 0.132$; females: $t_{40} = 0.520$, $P = 0.606$. **e** Excitatory synaptic drive, calculated as sEPSC frequency × sEPSC amplitude. 2xANOVA: sex x EtOH interaction ($F_{1,68} = 10.55$, **$P = 0.002$) but no main effects ($Ps > 0.05$); post hoc two-tailed unpaired t-tests with Holm-Sidak corrections show a sex difference between CON M and F ($t_{68} = 3.10$, *$P = 0.014$) and effect of EtOH in males ($t_{68} = 3.37$, **$P = 0.007$) but not females ($P > 0.50$). **f** sIPSC frequency. Two-tailed unpaired t-tests: males: $t_{28} = 1.48$, $P = 0.151$; females: $t_{40} = 0.02$, $P = 0.981$. **g** sIPSC amplitude. Two-tailed unpaired t-tests: males: $t_{28} = 1.16$, $P = 0.257$; females: $t_{40} = 1.02$, $P = 0.314$. **h** Inhibitory synaptic drive. 2xANOVA: no effects or interactions ($Ps > 0.30$). Data are presented as mean values + SEM.
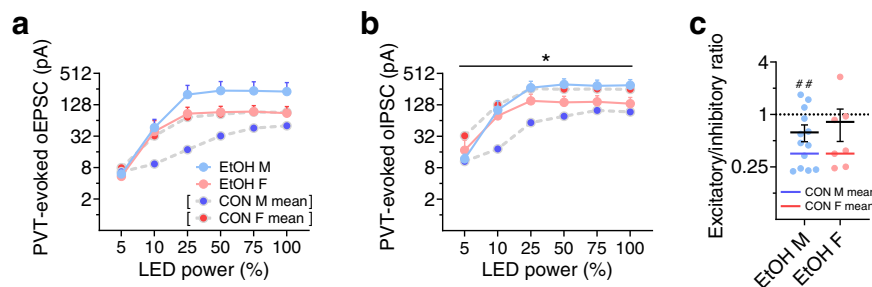

Fig. 7 A history of voluntary binge alcohol drinking induces a female-like phenotype in male PVT-BNST^CRF synapses. a–b Power-response curves for optically-evoked EPSCs (oEPSCs, **a**) and IPSCs (oIPSCs, **b**) in response to optical stimulation of ChR2 from PVT axon terminals. N's = 4 EtOH M, 12 cells and 3 EtOH F, 8 cells. Data in **a** and **b** are presented as mean values + SEM. Means for CON cell data in Fig. 3 are represented in this figure by blue and red lines for CON M and F, respectively. **a** 3xRM-ANOVA on oEPSCs: main effect of power ($F_{5,175} = 86.4$, $P < 0.0001$, not indicated) and a trend for an EtOH × power interaction ($F_{5,175} = 2.25$, $P = 0.052$), but no other effects or interactions ($Ps > 0.15$). **b** 3xRM-ANOVA on oIPSCs: main effect of power ($F_{5,175} = 103.4$, $P < 0.0001$, not indicated) and a sex × EtOH interaction ($F_{1,35} = 4.71$, *$P = 0.037$), but no other effects or interactions ($Ps > 0.05$). **c** oEPSC/oIPSC ratio in BNST^CRF neurons of EtOH mice. Data are presented as mean values ± SEM. EtOH M have E/I ratios below 1 (one-sample t-test: $t_{13} = 3.18$, $^{\#\#}P = 0.007$), which does not differ from that of CON M (two-tailed unpaired t-test: $t_{23} = 1.01$, $P = 0.321$). EtOH F does not have an E/I ratio below 1.0 (one-sample t-test: $t_6 = 1.71$, $P = 0.137$), however, this ratio does not significantly differ from CON F (two-tailed unpaired t-test: $t_{20} = 1.84$, $P = 0.081$).

a unique role for the PVT^BNST circuit in alcohol drinking that is independent of the role of the PVT in general appetitive reward.

In addition, we found that activation of the PVT^BNST pathway in aversive contexts, when BNST^CRF neuron activity is high[29,30], is sufficient to reduce avoidance behavior in both sexes, similar to the role of the BLA input in males[19]. These results suggest a critical sex-dependent role of this thalamo-limbic circuit in the control of and relationship between alcohol drinking and anxiety states. Further, repeated binge drinking produced a female-like phenotype in PVT-BNST^CRF synapses and BNST^CRF neurons in

males, characterized by increased excitation observed in naïve females and associated with greater binge drinking behavior. Notably, while the overall excitability phenotype becomes more similar to a female state, the mechanism(s) driving the alcohol-induced increase in excitability in males may be distinct from the underlying mechanisms of sex differences in excitability in the naïve population. However, our results provide a solid basis for future examination of the molecular similarities and differences between BNST^CRF neurons in males and females, as well as the effects of chronic alcohol. In addition, other glutamatergic inputs

and the BNST^CRF neuron population itself interact highly with other BNST neuron subpopulations, including PKCδ[33], neuropeptide Y[18], and dynorphin[20], among others. However, the literature is not yet comprehensive and provides some directly conflicting evidence regarding the independence and interactions between some BNST subpopulations. For example, one recent report suggests that the CRF and PKCδ populations in the male BNST receive direct synaptic input from the PVT and other regions as independent subpopulations that are inhibitory upon one another and modulate anxiety-like behavior in opposing manners (with CRF neurons being anxiogenic)[33]. In contrast, another recent study shows that these are highly overlapping populations and that acute stress recruits additional PKCδ expression in CRF neurons in females but not males[38], suggesting an important and perhaps sex-dependent function of the overlapping population of neurons. While both studies find that stress activates both types of neurons, they come to different conclusions about the organization and role(s) of these neurons in behavior. Further, BNST^CRF neurons are themselves complex, serving as both projection and interneurons[28]; as such, some may laterally inhibit others to participate in the polysynaptic inhibition we observed here. Altogether, our results and others point to the need for future studies to disentangle the independence, overlap, and interactions between BNST subpopulations, with special attention paid to the effects of sex and various physiological stressors (including alcohol and other drugs of abuse). Understanding the microcircuit organization and molecular makeup of these neurons is critical to defining the broader circuit architecture containing the PVT^VGLUT2-BNST^CRF circuit described here.

Methods

Subjects. All experimental mice were male and female adult mice on a C57BL/6J background strain. Wild-type C57BL/6J mice were purchased as adults from Jackson Laboratory, and all transgenic lines were bred in our animal facility. CRF-ires-Cre (CRF-Cre)[18,39] and VGLUT2-ires-Cre (VGLUT2-Cre)[40] mice were bred with WT C57BL/6J mice, and hemizygous CRF-Cre mice were bred with homozygous floxed Ai9-tdTomato or floxed EGFP-L10a mice purchased from Jackson Laboratory (stocks 007909 and 024750) to produce CRF-Cre-reporter mice. Mice were group-housed with ad libitum access to food and water in colony room on a 12:12 h reverse light cycle, with lights off at 7:30 a.m. Mice were singly housed for one week prior to the onset of behavioral experiments and remained singly housed thereafter. Experiments began approximately 3 h into the dark phase of the light cycle. All experimental procedures were approved by the Institutional Animal Care and Use Committees at Weill Cornell Medicine and the University of North Carolina-Chapel Hill.

Behavior assays. The standard Drinking in the Dark (DID) binge alcohol drinking paradigm was used in mice to model human binge consumption behavior[17]. For each cycle of EtOH DID, three hours into the dark cycle, the home cage water bottle was replaced with a bottle containing 20% (v/v) alcohol (EtOH) for two hours on Days 1–3 and four hours on Day 4, followed by three days of forced abstinence between consecutive cycles. A similar access schedule was used to evaluate binge sucrose consumption, except that home cage water bottles were replaced with 1% (w/v) sucrose. For all drinking experiments, empty "dummy" cages on the same rack as behavior mice received the same EtOH or sucrose bottle replacement, and consumption was adjusted for a leak from dummy bottles and then normalized to bodyweight. The open-field test (OF) was used to evaluate avoidance and locomotor behavior as previously performed[18]. Mice were placed in the 50 × 50 cm arena for 60 min, and Ethovision video tracking (Noldus, Wageningen, Netherlands) was used to quantify raw locomotor and location data used to calculate measures including distance traveled and time spent in each compartment (center vs. periphery, total). The elevated plus maze (EPM) was also used to assess anxiety-like behaviors and was conducted in a plexiglass maze with two open and two closed arms (35 cm length × 5.5 cm width, with walls 15 cm tall over the closed arms). Mice were placed in the center of the EPM for five-minute trials and movement and time spent in each compartment were tracked using SMART 2.0 and Ethovision 10 and 11. Total time and percent time spent in each arm were quantified.

Stereotaxic surgeries. For experiments requiring site-directed administration of viral vectors or retrobeads, mice were anesthetized with 2% isoflurane (VetEquip,

Livermore, CA) in 0.8% oxygen in an induction chamber (VetEquip, Livermore, CA) then placed in an Angle Two mouse stereotaxic frame (Leica Biosystems, Wetzlar, Germany) and secured with ear bars into a nose cone delivering isoflurane to maintain anesthesia. Mice were given a subcutaneous injection of meloxicam (2 mg/kg) for preemptive analgesia and 0.1 mL of 0.25% Marcaine around the incision site. A Neuros 7000 series 1 μL Hamilton syringe with a 33-gauge needle (Reno, NV) connected to a remote automated microinfusion pump (KD Scientific, Holliston, MA) was used for construct delivery at a rate of 50–100 nL/min to the PVT (A/P: −0.82, M/L: 0.00, D/V: −3.25, 200 nL) or BNST (A/P: +0.3 mm, M/L: ±1.1 mm, D/V: −4.35 mm, 250 nL). Following infusion, the needle was left in place for 10 min and then slowly manually retracted to allow for diffusion and prevent backflow of the virus. Mice were continuously monitored for at least 30 min post-surgery to ensure recovery of normal breathing pattern and sternal recumbency and then checked daily.

in vivo chemogenetic manipulations. To examine the role of PVT^VGLUT2 neurons in behavior, VGLUT2-Cre mice received a midline stereotaxic injection into the PVT of the kappa opioid receptor Gi-coupled DREADD (Gi-KORD) AAV9-hSyn-DIO-HA-KORD-IRES-mCitrine (gift from Bryan Roth) or control vector AAV8-hSyn-DIO-EYFP into the PVT (200 nL; Supplementary Fig. 4a). To examine the role of the PVT^BNST projection in binge alcohol drinking, binge sucrose drinking, and avoidance behavior, we used a multiplexed DREADD approach. C57BL/6J mice received injections of a retrograde Cre virus (AAVrg-hSyn-HI.EGFP-Cre.WPRE.SV40 or AAVrg-pmSyn1-EBFP-Cre) bilaterally in the BNST a midline PVT injection of either: (a) 1:1 cocktail of the excitatory Gq-DREADD AAV2-hSyn-DIO-hM3D(Gq)-mCherry (125 nL) plus inhibitory Gi-KORD AAV8-hSyn-DIO-KORD(Gi)-mCitrine (125 nL) or (b) control virus AAV2-hSyn-DIO-mCherry (250 nL, Fig. 5a, b). Approximately one week following surgery, mice started the DID procedure with a baseline cycle followed by a cycle in which they received 0.9% sterile saline vehicle (10 ml/kg, i.p.) injections on Days 2 and 4 forty min prior to alcohol access to habituate to the injection procedure. Chemogenetic manipulations began the next cycle with saline on Day 2 and clozapine-n-oxide (CNO, 5 mg/kg in 0.9% saline) on Day 4. The Gi-KORD was subsequently evaluated similarly with a DMSO vehicle (1 ml/kg, s.c.) injection cycle and manipulation cycle with Salvinorin B (SalB, 17 mg/kg in DMSO). Mice displaying injection stress defined by >1 g/kg reduction in and <1 g/kg vehicle baseline drinking were excluded from the analysis. For the OF and EPM, half of the animals of each sex received the vehicle and half received the DREADD activator (CNO or SalB) 40 min prior to the assay. For sucrose DID, the same SalB or CNO drug administration procedure was used as that for EtOH DID.

Brain extraction and fluorescence immunohistochemistry. Following behavior procedures, mice were deeply anesthetized with pentobarbital (100 mg/kg, i.p.) and transcardially perfused with sterile phosphate-buffered saline (PBS) followed by 4% paraformaldehyde (PFA). Brains were extracted, post-fixed overnight in 4% PFA, and then placed in PBS until they were sliced on the coronal plane in 45 μm sections on a VT1000S vibratome (Leica Biosystems) to check injection placements and viral expression (hit maps of these expression data are presented in Supplementary Fig. 7a, b). To amplify the expression of fluorophore tags, coronal slices containing the PVT and BNST from DREADD and CON mouse brains underwent immunofluorescence staining. Slices were washed twice in PBS followed by 0.2% triton (Fisher Bioreagents, Hampton, NH) for 10 min each and then blocked in 5% normal donkey serum (NDS) for 30 min. Tissue was incubated in primary antibody (DsRed rabbit polyclonal 1:400, Takara, Kusatsu, Japan) overnight at room temperature. The next day, slices were washed 3 times in 0.2% triton for 10 min each and then blocked in 5% NDS for 30 min. Tissue was then incubated in secondary antibody (Alexafluor-568 donkey anti-rabbit, 1:250, Invitrogen, Carlsbad, CA) for 2 h and subsequently washed twice in 0.2% Triton and then in PBS for 10 min each. Slices were counterstained with DAPI and mounted on slices, and coverslipped with Vectashield hard mount antifade mounting medium (Vector Labs, Burlingame, CA), and stored in the dark at 4 °C until imaged (as described below) to verify surgical placements and viral expression.

Retrograde neuronal tracing. For anatomical circuit tracing of excitatory inputs to the BNST, VGLUT2-Cre mice received stereotaxic injections of a retrograde virus (AAVrg-Ef1a-DO-DIO-TdTomato_EGFP-WPRE-pA) unilaterally into the BNST, which was is retrogradely trafficked to ultimately express GFP in Cre+ cells and tdTomato in Cre− cells that project to the BNST. Following three weeks to allow for optimal viral expression, mice were sacrificed and their brains harvested for quantification.

Image acquisition and analysis. Coronal brain slices were collected and imaged for all experiments to confirm and quantify viral expression and immunolabeling. Images were acquired on a Zeiss LSM 880 Laser Scanning Confocal microscope (Carl Zeiss, Oberkochen, Germany). For the retrograde tracing experiment, images of the PVT and BLA were quantified using ImageJ 1.50 (US National Institute of Health) to count the total number of DAPI-stained nuclei, GFP+, and tdTomato+ cells. The coordinates of each cell were analyzed using a custom MATLAB (MathWorks, Natick, MA) program and normalized to the most dorsomedial point

of the PVT. Heatmaps of the density of BNST-projecting neurons were generated as described elsewhere[41], overlaying data from four mice per sex. The proportion of PVT projectors that are VGLUT2+ was calculated as GFP+/(GFP + plus tdTomato+). Coordinates analyzed (mm from Bregma): BLA (−1.55), anterior (aPVT, −0.46 mm), anterior-mid (am-PVT, −0.70), mid (mPVT, −1.22), and posterior (pPVT, −1.91).

ex vivo slice electrophysiology and calcium imaging. Slice electrophysiology experiments were performed as previously conducted in our laboratory[9,18]. Mice were decapitated under isoflurane anesthesia and their brains were rapidly extracted. Coronal BNST slices (300 µm) were prepared on a VT1200 vibratome (Leica Biosystems) in ice-cold, oxygenated (95% O_2/5% CO_2) sucrose artificial cerebrospinal fluid (aCSF) containing (in mM): 194 sucrose, 20 NaCl, 4.4 KCl, 2 CaCl2, 1 Mg Cl2, 1.2 NaH2PO4, 10 glucose, and 26 NaHCO3 (pH 7.3 and 30 mOsm). Slices were transferred to a holding chamber with 30 °C oxygenated normal aCSF (in mM):124 NaCl, 4.4 KCl, 2 CaCl2, 1.2 MgSO4, 1 NaH2PO4, 10 glucose, and 26 NaHCO3 (pH 7.3 and 30 mOsm) and allowed to equilibrate for at least one hour. For electrophysiological recordings, slices were transferred to a submerged recording chamber (Warner Instruments, Hamden, CT) and perfused at a rate of 2 mL/min with 30 °C oxygenated normal aCSF.

BNST[CRF] neurons were identified for recording with their tdTomato tag using a 580 nm LED under 40x objective (Olympus, Tokyo, Japan). Signals were acquired using a Multiclamp 700B amplifier (Molecular Devices), digitized, and analyzed via pClamp 10 software (Molecular Devices). Input resistance and access resistance were continuously monitored throughout experiments, and cells in which access resistance changed by more than 20% were not included in data analysis. Excitability experiments were performed in current-clamp configuration using a potassium gluconate-based intracellular recording solution containing (in mM): 135 KGluc, 5 NaCl, 2 $MgCl_2$−6H2O, 10 HEPES, 0.6 EGTA, 4 Na-ATP and 0.4 Na-GTP (pH 7.3 and 290 mOsm). Synaptic transmission was measured in the voltage-clamp configuration using a cesium-methanesulfonate-based intracellular recording solution containing (in mM): 135 CsMeth, 10 KCl, 10 HEPES, 1 $MgCl_2$·6H2O, 0.2 EGTA, 4 Mg-ATP, 0.3 Na2GTP, 20 phosphocreatine (pH 7.3, 290 mOsm) and driving force (−55 mV and +10 mV) to isolate excitatory and inhibitory transmission within individual neurons. Miniature postsynaptic currents were measured in the presence of tetrodotoxin (TTX, 1 µM) in the aCSF bath. Paired pulse ratio and AMPA/NMDA ratio were assessed using a cesium gluconate-based intracellular recording solution containing (in mM): 117 D-gluconic acid, 20 HEPES, 0.4 EGTA, 5 TEA, 2 $MgCl_2$-6H2O, 4 Na-ATP, and 0.4 Na-GTP (pH 7.3 and 290 mOsm), at a holding potential of −70 mV, and with picrotoxin (25 µM) in the aCSF bath.

Prior to slice electrophysiology experiments, mice underwent three cycles of EtOH DID (EtOH group) or a water control DID procedure in which the replacement bottle contained water instead of EtOH (CON group) to allow for investigation of basic sex differences in function, as well as for direct comparison to EtOH mice. Twenty-four hours following the onset of the last EtOH or water bottle access, mice were sacrificed for slice electrophysiology experiments as described above. For experiments investigating PVT[BNST] neurons, mice received bilateral intra-BNST injections of green or red retrobeads (250 nL, Lumafluor) prior to DID to label this population for identification during recordings. For experiments characterizing postsynaptic responses in BNST[CRF] neurons to PVT glutamate inputs, mice received an intra-PVT stereotaxic injection of AAV5-CamKIIα-hChR2(H134R)-eYFP.WPRE.hGH (200 nL, Penn Vector Core and Addgene) three weeks prior to DID procedures. During recordings, 1 ms 490 nm LED stimulation was used to optically stimulate ChR2 + PVT cell bodies to elicit action potentials to confirm sufficient PVT expression and ChR2 fidelity at 1, 2, 5, 10, 20, and 50 Hz. One 2 ms stimulation every 10 s was used in the BNST to optically-evoke glutamate release from PVT terminals while recording postsynaptic responses (oPSCs) from BNST[CRF] neurons in voltage-clamp, and 2 ms stimulation at 1, 2, 5, 10, and 20 Hz was used while measuring postsynaptic potentials (oPSPs) in BNST[CRF] neurons in current-clamp. Polysynaptic and monosynaptic oPSCs were assessed with the bath application of TTX (500 nM) to block all neurotransmission followed by the addition of 4-aminopyridine (100 µM) to reinstate monosynaptic transmission.

Following behavior, a subset of PVT[BNST] DREADD mice were sacrificed for slice electrophysiology confirmation of the approach using bath application of CNO (10 µM) during current-clamp recordings of DREADD + PVT cell bodies in the presence of TTX (Supplementary Fig. 7c). To provide confirmation of the approach at the BNST[CRF] neuron population level, CRF-Cre mice received bilateral intra-BNST injections of the calcium sensor GCaMP6s (AAV4-Syn-FLEX-GCaMP6s; UPenn Vector Core; 500 nL) and an intra-PVT injection of the excitatory hM3D DREADD virus (AAV2-CaMKIIα-hM3D(Gq)-mCherry, 200 nL) or control virus (AAV8-CaMKIIα-mCherry; Supplementary Fig. 7d). Four weeks later, fresh brain slices were acutely prepared as described for slice electrophysiology recordings above. GCaMP6s was excited with 35% 470 nm LED (CoolLED) at a frequency of 1 Hz for 10 s every min to minimize photobleaching, and videos were acquired at a frame rate of 10 Hz with an optiMOS monochrome camera (QImaging, Surrey, British Columbia, Canada) and MicroManager 1.4 software, across the entire experiment including a five min baseline, 10 min bath application of CNO (10 µM), and 10 min washout period. The experimenter

maintained an objective to focus on the BNST z-plane of interest containing several CRF[GCaMP6s] neurons throughout the experiment. Custom code (MATLAB 9.4) was used to analyze changes in fluorescence intensity in individual CRF[GCaMP6] neurons (ΔF) compared to background fluorescence within the frame (intensity of the entire field of view, F) throughout the video. CRF[GCaMP6s] cells from CON virus mice were used to quantify the inherent linear decay in fluorescence of GCaMP6s, and fluorescence in hM3D CRF[GCaMP6s] cell fluorescence was normalized to this decay for statistical analysis.

Statistical analyses. Statistical analyses were performed in GraphPad Prism 8. Data for all dependent measures were examined for their distributions in normal and log space, outliers, and equality of variance across groups using Q-Q plots. Electrophysiological properties (except I_h and membrane potential) and synaptic transmission data were lognormally distributed, analyzed using log-transformed values, and presented as raw values on a log2 scale in figures; all other data were normally distributed, analyzed in raw space, and presented on a linear scale in figures. Outliers according to Q–Q plots were excluded (however this was rare and reported). Data are presented as mean ± SEM, and raw data points are included in all figures except those with more than two repeated measures when there were too many raw data points to be clearly represented.

Two-way analysis of variance (ANOVA) and unpaired t-tests were used to evaluate the effects of sex and alcohol on synaptic transmission and excitability data. Repeated measures ANOVAs (RM-ANOVAs) were used to examine the effects of treatment, cycles of binge drinking, different anatomical subregions, etc., within individual animals across experimental groups; mixed-effects models were used when one or more matched data points was unavailable for an individual animal. To prevent false-positive results and overinterpretation of RM-ANOVAs on behavioral data, sphericity was not assumed and the Geisser and Greenhouse correction of degrees of freedom was employed for the repeated measure. For all ANOVAs, significant effects were further probed with appropriate post hoc paired or unpaired t-tests with Holm–Sidak correction for multiple comparisons, and multiplicity-adjusted P values are reported. Differences in proportions between groups were assessed with Fisher's exact tests, and differences within the group from a null hypothesis value were evaluated using one-sample t-tests. Statistical comparisons were always performed with an alpha level of 0.05 and using two-tailed analyses.

Reporting summary. Further information on research design is available in the Nature Research Reporting Summary linked to this article.

Data availability
All data generated for this study are available on Figshare (https://doi.org/10.6084/m9.figshare.c.5517420.v2). Source data are provided with this paper.

Code availability
Custom MATLAB code used in this study is available on Figshare along with the raw data (https://doi.org/10.6084/m9.figshare.c.5517420.v2). Source data are provided with this paper.

References
1. Kessler, R. C. et al. Lifetime co-occurrence of DSM-III-R alcohol abuse and dependence with other psychiatric disorders in the National Comorbidity Survey. *Arch. Gen. Psychiatry* **54**, 313–321 (1997).
2. McHugh, R. K., Votaw, V. R., Sugarman, D. E. & Greenfield, S. F. Sex and gender differences in substance use disorders. *Clin. Psychol. Rev.* **66**, 12–23 (2018).
3. Piazza, N. J., Vrbka, J. L. & Yeager, R. D. Telescoping of alcoholism in women alcoholics. *Int. J. Addict.* **24**, 19–28 (1989).
4. Satta, R., Hilderbrand, E. R. & Lasek, A. W. Ovarian hormones contribute to high levels of binge-like drinking by female mice. *Alcohol Clin. Exp. Res.* **42**, 286–294 (2018).
5. Sneddon, E. A., White, R. D. & Radke, A. K. Sex differences in binge-like and aversion-resistant alcohol drinking in C57BL/6J mice. *Alcohol Clin. Exp. Res.* **43**, 243–249 (2019).
6. Radke, A. K., Sneddon, E. A., Frasier, R. M. & Hopf, F. W. Recent perspectives on sex differences in compulsion-like and binge alcohol drinking. *Int. J. Mol. Sci.* **22**, https://doi.org/10.3390/ijms22073788 (2021).
7. Avery, S. N., Clauss, J. A. & Blackford, J. U. The human BNST: functional role in anxiety and addiction. *Neuropsychopharmacology* **41**, 126–141 (2016).
8. Avery, S. N. et al. BNST neurocircuitry in humans. *NeuroImage* **91**, 311–323 (2014).

9. Pleil, K. E. et al. Effects of chronic ethanol exposure on neuronal function in the prefrontal cortex and extended amygdala. *Neuropharmacology* **99**, 735–749 (2015).

10. Rinker, J. A. et al. Extended amygdala to ventral tegmental area corticotropin-releasing factor circuit controls binge ethanol intake. *Biol. Psychiatry* https://doi.org/10.1016/j.biopsych.2016.02.029 (2016).

11. Millan, E. Z., Ong, Z. & McNally, G. P. Paraventricular thalamus: gateway to feeding, appetitive motivation, and drug addiction. *Prog. Brain Res.* **235**, 113–137 (2017).

12. Hua, R. et al. Calretinin neurons in the midline thalamus modulate starvation-induced arousal. *Curr. Biol.* **28**, e3944 (2018).

13. Huang, A. S., Mitchell, J. A., Haber, S. N., Alia-Klein, N. & Goldstein, R. Z. The thalamus in drug addiction: from rodents to humans. *Philos. Trans. R. Soc. London* **373**, https://doi.org/10.1098/rstb.2017.0028 (2018).

14. Kirouac, G. J. Placing the paraventricular nucleus of the thalamus within the brain circuits that control behavior. *Neurosci. Biobehav. Rev.* **56**, 315–329 (2015).

15. Bava, S., Jacobus, J., Thayer, R. E. & Tapert, S. F. Longitudinal changes in white matter integrity among adolescent substance users. *Alcohol. Clin. Exp. Res.* **37**, E181–E189 (2013).

16. Rhodes, J. S., Best, K., Belknap, J. K., Finn, D. A. & Crabbe, J. C. Evaluation of a simple model of ethanol drinking to intoxication in C57BL/6J mice. *Physiol. Behav.* **84**, 53–63 (2005).

17. Thiele, T. E., Crabbe, J. C. & Boehm, S. L. 2nd Drinking in the Dark” (DID): a simple mouse model of binge-like alcohol intake. *Curr. Protoc. Neurosci.* **68**, 9.49.41–12 (2014).

18. Pleil, K. E. et al. NPY signaling inhibits extended amygdala CRF neurons to suppress binge alcohol drinking. *Nat. Neurosci.* **18**, 545–552 (2015).

19. Kim, S. Y. et al. Diverging neural pathways assemble a behavioural state from separable features in anxiety. *Nature* **496**, 219–223 (2013).

20. Crowley, N. A. et al. Dynorphin controls the gain of an amygdalar anxiety circuit. *Cell Rep.* **14**, 2774–2783 (2016).

21. Dong, X., Li, S. & Kirouac, G. J. Collateralization of projections from the paraventricular nucleus of the thalamus to the nucleus accumbens, bed nucleus of the stria terminalis, and central nucleus of the amygdala. *Brain Struct. Funct.* **222**, 3927–3943 (2017).

22. Penzo, M. A. et al. The paraventricular thalamus controls a central amygdala fear circuit. *Nature* **519**, 455–459 (2015).

23. Zhu, Y., Wienecke, C. F., Nachtrab, G. & Chen, X. A thalamic input to the nucleus accumbens mediates opiate dependence. *Nature* **530**, 219–222 (2016).

24. Keyes, P. C. et al. Orchestrating opiate-associated memories in thalamic circuits. *Neuron* https://doi.org/10.1016/j.neuron.2020.06.028 (2020).

25. Vardy, E. et al. A new DREADD facilitates the multiplexed chemogenetic interrogation of behavior. *Neuron* **86**, 936–946 (2015).

26. Reed, S. J. et al. Coordinated reductions in excitatory input to the nucleus accumbens underlie food consumption. *Neuron* **99**, 1260–1273.e1264 (2018).

27. Neumann, P. A. et al. Cocaine-induced synaptic alterations in thalamus to nucleus accumbens projection. *Neuropsychopharmacology* **41**, 2399–2410 (2016).

28. Marcinkiewcz, C. A. et al. Serotonin engages an anxiety and fear-promoting circuit in the extended amygdala. *Nature* **537**, 97–101 (2016).

29. Salimando, G. J., Hyun, M., Boyt, K. M. & Winder, D. G. BNST GluN2D-containing NMDA receptors influence anxiety- and depressive-like behaviors and modulate cell-specific excitatory/inhibitory synaptic balance. *J. Neurosci.* https://doi.org/10.1523/jneurosci.0270-20.2020 (2020).

30. Silberman, Y. & Winder, D. G. Emerging role for corticotropin releasing factor signaling in the bed nucleus of the stria terminalis at the intersection of stress and reward. *Front. Psychiatry* **4**, 42 (2013).

31. Silberman, Y., Matthews, R. T. & Winder, D. G. A corticotropin releasing factor pathway for ethanol regulation of the ventral tegmental area in the bed nucleus of the stria terminalis. *J. Neurosci.* **33**, 950–960 (2013).

32. Vranjkovic, O., Pina, M., Kash, T. L. & Winder, D. G. The bed nucleus of the stria terminalis in drug-associated behavior and affect: a circuit-based perspective. *Neuropharmacology* **122**, 100–106 (2017).

33. Wang, X. et al. Anxiety-related cell-type-specific neural circuits in the anterior-dorsal bed nucleus of the stria terminalis. *Sci. Bull.* **65**, 1203–1216 (2020).

34. Do-Monte, F. H., Quiñones-Laracuente, K. & Quirk, G. J. A temporal shift in the circuits mediating retrieval of fear memory. *Nature* **519**, 460–463 (2015).

35. Do-Monte, F. H., Minier-Toribio, A., Quiñones-Laracuente, K., Medina-Colón, E. M. & Quirk, G. J. Thalamic regulation of sucrose seeking during unexpected reward omission. *Neuron* **94**, 388–400.e384 (2017).

36. Choi, E. A. & McNally, G. P. Paraventricular thalamus balances danger and reward. *J. Neurosci.* **37**, 3018–3029 (2017).

37. Otis, J. M. et al. Paraventricular thalamus projection neurons integrate cortical and hypothalamic signals for cue-reward processing. *Neuron* **103**, 423–431.e424 (2019).

38. Fetterly, T. L. et al. α2A-adrenergic receptor activation decreases parabrachial nucleus excitatory drive onto BNST CRF neurons and reduces their activity in vivo. *J. Neurosci.* **39**, 472–484 (2019).

39. Krashes, M. J. et al. An excitatory paraventricular nucleus to AgRP neuron circuit that drives hunger. *Nature* **507**, 238–242 (2014).

40. Vong, L. et al. Leptin action on GABAergic neurons prevents obesity and reduces inhibitory tone to POMC neurons. *Neuron* **71**, 142–154 (2011).

41. Beyeler, A. et al. Organization of valence-encoding and projection-defined neurons in the Basolateral Amygdala. *Cell Rep.* **22**, 905–918 (2018).

Acknowledgements

Author contributions

K.E.P. designed all experiments, O.B.L., M.J.S., and K.E.P. collected and analyzed slice electrophysiology data, O.B.L., J.D.M., J.F.D., S.A.R., J.K.R.I., J.A.R., and K.E.P. performed and analyzed behavior data. J.D.M. collected and analyzed anatomical tracing data, and J.F.D. and J.D.M. bred mice for all studies. K.E.P., T.R.T., and T.L.K. oversaw experiments. K.E.P. and O.B.L. wrote the manuscript, and all authors edited and approved the final version of the manuscript.

Competing interests

The authors declare no competing interests.

Additional information

Supplementary information The online version contains supplementary material available at https://doi.org/10.1038/s41467-021-25368-y.

Correspondence and requests for materials should be addressed to K.E.P.

Peer review information *Nature Communications* thanks Jacqueline Barker, Mario Penzo and the other, anonymous, reviewer(s) for their contribution to the peer review of this work.

Reprints and permission information is available at http://www.nature.com/reprints

Publisher's note Springer Nature remains neutral with regard to jurisdictional claims in published maps and institutional affiliations.